RESEARCH ARTICLE | JUNE 10 2025

# Identifying high-energy electronic states of NV<sup>-</sup> centers in diamond

**Special Collection: Defects in Solids for Quantum Technologies** 

Minh Tuan Luu ⑩ ; Christopher Linderälv; Zsolt Benedek; Ádám Ganyecz ⑩ ; Gergely Barcza ⑩ ; Viktor Ivády ⑩ ; Ronald Ulbricht ➡ ⑪



Appl. Phys. Lett. 126, 234001 (2025) https://doi.org/10.1063/5.0268247





# Articles You May Be Interested In

Narrow inhomogeneous distribution of spin-active emitters in silicon carbide

Appl. Phys. Lett. (April 2021)

Elucidating the local atomic and electronic structure of amorphous oxidized superconducting niobium films

Appl. Phys. Lett. (December 2021)

Variational simulation of Schwinger's Hamiltonian with polarization qubits

Appl. Phys. Lett. (April 2021)





# Identifying high-energy electronic states of NV<sup>-</sup> centers in diamond ••

Cite as: Appl. Phys. Lett. **126**, 234001 (2025); doi: 10.1063/5.0268247 Submitted: 28 February 2025 · Accepted: 26 May 2025 · Published Online: 10 June 2025







Minh Tuan Luu, <sup>1</sup> (1) Christopher Linderälv, <sup>2</sup> Zsolt Benedek, <sup>3,4</sup> Ádám Ganyecz, <sup>4,5</sup> (1) Gergely Barcza, <sup>4,5</sup> (1) Viktor Ivády, <sup>3,4,a</sup> (1) and Ronald Ulbricht (1)

#### **AFFILIATIONS**

- <sup>1</sup>Max-Planck Institut für Polymerforschung, Ackermannweg 10, 55128 Mainz, Germany
- <sup>2</sup>Department of Physics, Centre for Material Science and Nanotechnology, University of Oslo, P.O. Box 1048, Blindern, Oslo N-0316, Norway
- <sup>3</sup>Department of Physics of Complex Systems, Eötvös Loránd University, Egyetem tér 1-3, H-1053 Budapest, Hungary
- <sup>4</sup>MTA-ELTE Lendület "Momentum" NewQubit Research Group, Pázmány Péter, Sétány 1/A, 1117 Budapest, Hungary

Note: This paper is part of the Special Topic, Defects in Solids for Quantum Technologies.

#### **ABSTRACT**

The negatively charged nitrogen-vacancy center in diamond is a prototype photoluminescent point defect spin qubit with promising quantum technology applications, enabled by its efficient optical spin polarization and readout. Its low-lying electronic states and optical spin polarization cycle have been well characterized over decades, establishing it as a benchmark system for state-of-the-art computational methods in point defect research. While the optical cycle is well understood, a comprehensive energetic analysis of higher-lying states has received less attention until recently. In this joint experimental theoretical study, we identify and characterize five high-energy states beyond those involved in the optical cycle. Using transient absorption spectroscopy, we determine their transition energies and relative oscillator strengths. Additionally, we perform two independent numerical studies employing two state-of-the-art post-density functional theory methods to support the experimental findings and assign energy levels. These results enhance our understanding of the nitrogen-vacancy center's energy spectrum, providing a broader reference for benchmarking high-level first-principles methods.

© 2025 Author(s). All article content, except where otherwise noted, is licensed under a Creative Commons Attribution (CC BY) license (https://creativecommons.org/licenses/by/4.0/). https://doi.org/10.1063/5.0268247

Nitrogen-vacancy (NV) centers in diamond<sup>1</sup> have emerged as a promising platform for quantum sensing<sup>2–4</sup> and quantum information processing.<sup>5</sup> The negatively charged state (NV<sup>-</sup>) is of particular interest due to its long spin coherence time at room temperature<sup>6</sup> and the ability to optically initialize and readout spin states, <sup>1</sup> allowing measurements of physical quantities such as electromagnetic fields, <sup>7</sup> temperature, <sup>8</sup> and mechanical strain.<sup>9</sup> Additionally, nearby nuclear spins enable the implementation of small-scale quantum computing circuits, while the NV<sup>-</sup> center implemented spin-photon interfaces, and quantum repeaters hold promise for building quantum networks.

The spin-dependent optical excitation cycle, which enables optical initialization and readout, is governed by the low-lying electronically excited states of NV<sup>-</sup>. These states, along with their optical and spin-orbit coupling, have been thoroughly studied, leading to a solid

understanding of the spin polarization mechanism and the spin-dependent photoluminescence signal,  $^{10}$  making this defect has become a benchmark system for state-of-the-art theoretical methods.  $^{11-26}$  Higher-lying excited states, which can play a role in photoionization and photoelectric readout of NV $^{-27}$  as well as extend the scope for theoretical benchmarking, have received much less attention.

Recently, we experimentally discovered a range of high-energy excited states using transient absorption (TA) spectroscopy. <sup>28,29</sup> Our results also provided direct evidence of electron transfer from NV<sup>-</sup> to nearby nitrogen defects, explaining photoluminescence quenching and its dependence on nitrogen concentration. <sup>28</sup> Theoretical predictions for high-energy states have been scarce, <sup>19,30–34</sup> making their identification difficult. This is also because standard computational methods have difficulties in dealing with excited states, especially those beyond

<sup>&</sup>lt;sup>5</sup>HUN-REN Wigner Research Centre for Physics, P.O. Box 49, H-1525 Budapest, Hungary

a) Electronic mail: ivady.viktor@ttk.elte.hu

b) Author to whom correspondence should be addressed: ulbricht@mpip-mainz.mpg.de

the first excited state that are potentially resonant with the conduction band (CB). The situation has improved with the development of new post-density functional theory (DFT) methods that can simultaneously account for the static correlation of the localized defect states and the screening effect of the embedding host electron states.<sup>35</sup>

In this Letter, we further investigate the newly observed excited state by experimentally determining the relative transition strengths and conducting state-of-the-art numerical simulations using two independent methods to identify and label features of the high-energy spectra.

A two-pump femtosecond TA setup was implemented to measure the excited electronic states of NV in both the triplet and singlet spin channels, as shown schematically in Fig. 1(a). The first pump has a photon energy of 2.4 eV (515 nm), followed by a second pump at 1.38 eV (900 nm) arriving 15 ns later. The white-light (WL) probe beam is generated in a 4 mm c-cut sapphire crystal, with a spectrum covering either the 1.5-3.3 eV range (2.4 eV input, for higher excited states measurements) or the 1.1-2.3 eV range (1.07 eV input, for lower singlet states measurements). We probe the change in the transmission of the WL pulse ( $\Delta$  T/T) under excitation, where  $\Delta$  T/T > 0 indicates either ground state bleaching (GSB) or stimulated emission (SE) from the excited state, while  $\Delta T/T < 0$  signifies excited state absorption (ESA). To probe the triplet channel, the WL measures  $\Delta$  T/T 5 ps after the first pump (2.4 eV). To measure the singlet channel, the system is allowed to relax after 2.4 eV excitation for 15 ns, so that population has either decayed to  ${}^{3}A_{2}$  or  ${}^{1}E$ . The second pump at 1.38 eV then excites the  ${}^{1}E \rightarrow {}^{1}A_{1}$  transition, with the white-light probing  $\Delta$  T/T 5 ps later.

We used high-pressure high-temperature (HPHT) diamonds that contain about 2 ppm of NV $^-$  with a high concentration of single-substitutional nitrogen  $N_s~(\sim 100\, ppm)$  to minimize the presence of NV $^0$ . All measurements were performed at a temperature of 10 K. Details of the experimental setup were previously published.  $^{28}$ 

To theoretically describe the observed high-energy states, two approaches were used: (i) complete active space self-consistent field (CASSCF) method, <sup>36–38</sup> followed by 2nd-order N-electron valence state perturbation theory (NEVPT2) <sup>39–41</sup> method on hydrogenterminated nanodiamonds; (ii) constrained random phase and full-configurational interaction (cRPA+FCI) calculations <sup>17,42</sup> on supercells.

The first methodology is similar to that described in detail in our previous work.<sup>26</sup> The used nanodiamonds, labeled as MODEL-I, MODEL-II, and MODEL-III, contain 34, 70, and 164 C atoms and differ from our previous models<sup>26</sup> by that they are expanded to reduce the steric clash among terminal H atoms.

State-average (SA) CASSCF calculations, followed by NEVPT2, were performed with the 4 defect-localized bandgap orbitals and six electrons in the active space, with five triplet and eight singlet eigenstates. We applied the cc-pVDZ (double-zeta)<sup>43</sup> basis set along with def2/J<sup>44</sup> and cc-pVDZ/C<sup>45</sup> auxiliary sets for density fitting approximations. The cluster geometries were optimized to the ground triplet ( $^3A_2$ ) electronic state also with CASSCF. CASSCF-NEVPT2 calculations were carried out using ORCA 6.0.1. See the supplementary material (SI), section S1.4 for sample input files. Here, results with MODEL-III are presented, and further results with smaller models are also in the SI.

The second method is using DFT and constrained random phase approximation (cRPA) to parameterize a Hamiltonian that can be solved using full configuration interaction (FCI). This method was demonstrated for the low-energy states of the  $\mathrm{NV}^{-1}$  center recently. The cRPA+FCI calculations<sup>17</sup> were performed as outlined in Ref. 42 using the Vienna Ab initio Simulation Package, VASP, 52,53 and an inhouse implementation of configuration interaction. Here, the lattice parameter was 3.57 Å, and a  $3 \times 3 \times 3$  repetition of the unit cell was used for modeling the defect, consisting of 216 atoms. The exchange-correlation functional used was HSE06 (Heyd-Scuseria-Ernzerhof). The Brillouin zone was sampled at the  $\Gamma$ -point only, and the plane wave basis was truncated at 520 eV. In the cRPA<sup>56</sup> calculation, four localized (spin paired) states were used, and empty states with energies up to 36 eV above the CB were included. The one-body matrix elements were obtained from orbital energy levels with Hartree double counting correction.<sup>42</sup>

Figure 1 shows the energy scheme of the electronic states and optical transitions in both the singlet and triplet channels. Exciting electrons from  ${}^3A_2$  to  ${}^3E$  using a 2.4 eV pump revealed an ESA feature at 2.38 eV (520 nm) whose relaxation dynamics matched that of the SE signal from the  ${}^3E$  state, indicating that the ESA signal observed is a spin-triplet state above  ${}^3E$  and was attributed to the  ${}^3E'$  state. This  ${}^3E'$  state also appeared in photoluminescence excitation

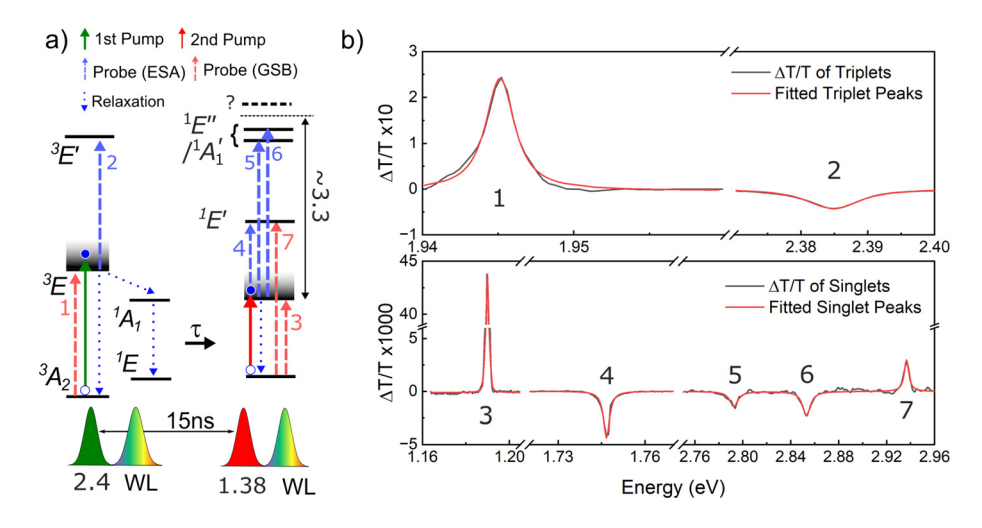


**FIG. 1.** (a) Schematic energy level structure and scheme of the TA measurements in triplet and singlet channels. Probe energy is limited to 3.3 eV from  $^1A_1$ . (b) Fitted curves of baseline-subtracted TA signal of transitions involving high-energy states in NV $^-$ . Top: triplet channel; bottom: singlet channel. Fit values are detailed in Table I

**TABLE I.** Summary of observed transition peak properties (Fig. 1b) compared to CASSCF-NEVPT2 (theory 1) and CRPA+FCI (theory 2) results. Transition energies are in eV, and full-width-half-maximum (FWHM) of the experimental peaks (in square brackets) are measured in meV. Oscillator strengths of the singlet and the triplet systems are normalized to the corresponding ZPL cross sections.

Peak	Transition	Energy (eV)			Oscillator strength			DW (%)
		Exp.	Theory 1	Theory 2	Exp.	Theory 1	Theory 2	Exp.
1	$^3A_2 \rightarrow {}^3E$	1.945 [1.4]	2.11	2.20	1 <sup>a</sup>	1		3.2 <sup>62,63</sup>
2	${}^3E \rightarrow {}^3E^{\prime}$	2.385 [7.7]	2.22	2.35	0.49	0.54		8.1 <sup>28</sup>
3	$^1E  ightarrow  ^1A_1$	1.19 [1.4]	1.02	0.88	1	1		$41^{63}$
4	$^{1}A_{1} ightarrow{}^{1}E^{^{\prime}}$	1.75 [3.3]	1.71	1.82	0.22	0.04		42 <sup>28</sup>
5	${}^{1}A_{1} \rightarrow {}^{1}E^{''}/{}^{1}A_{1}^{'}$	2.79 [6.9]	2.89	3.61	0.01	0.10		
6	${}^{1}A_{1} \rightarrow {}^{1}E^{''}/{}^{1}A_{1}^{'}$	2.85 [8.1]	2.35	3.77	0.02	1.14		
7	$^{1}E \rightarrow {}^{1}E^{'}$	2.94 [4.7]	2.73	2.70	0.01	0.10		

<sup>&</sup>lt;sup>a</sup>Intensity halved assuming GSB and SE give equal contributions.

(PLE) measurements<sup>57</sup> as a reduction of the NV<sup>-</sup> PL signal and an increase in NV<sup>0</sup> signal, hinting toward a charge conversion process as the <sup>3</sup>E' got excited.

For the singlet system, the TA spectrum reveals several absorption peaks at 1.75, 2.79, and 2.85 eV that share the relaxation lifetime of 130 ps of the  $^1A_1$  state.  $^{28,58}$  The spectrum also shows the  $^1E \rightarrow ^1E'$  transition at 2.94 eV as GSB. Although 1.75 eV has been predicted before  $^{32,59,60}$  and experimentally verified along with a GSB replica at 2.94 eV,  $^{28}$  the higher energy singlet states have neither been theoretically considered nor concretely observed experimentally. Due to the rapidly diminishing probe sensitivity toward the UV region, any potential transition located 3.3 eV above  $^1A_1$  cannot be identified.

All zero-phonon line (ZPL) peaks were fitted with Lorentzian functions, giving their spectral positions, linewidth, and relative intensity. The intensity of the peaks in the triplet or singlet channel was normalized to the transition between the two lowest states in each system ( ${}^3A_2 \rightarrow {}^3E$  for triplets and  ${}^1E \rightarrow {}^1A_1$  for singlets). The results of the peak fitting are summarized in Table I alongside the values from theoretical models. Due to the low intensity of the higher singlet state peaks, the phonon sideband of such transitions could not be observed. The intensity of the peaks at the ZPLs comprises both the GSB and SE signals. However, this was only relevant in the  ${}^3A_2 \rightarrow {}^3E$  transition since the SE signal for this transition was comparable to the GSB signal. For other transitions, the SE signals were extremely low compared to the GSB signal or simply not detectable, thus excluded in the oscillator strength values.

We start the theoretical considerations by discussing the possible nature of high-energy states using group theory, based on the orbital energy diagram of the NV<sup>-</sup> center (see Fig. 2). There are four defect-localized orbitals in the vicinity of the bandgap, formed by the superposition of four dangling atomic 2p orbitals around the vacancy. Using notations corresponding to the  $C_{3\nu}$  symmetry, we have two half-occupied degenerate e orbitals and two occupied  $a_1$  orbitals ( $a_1$  and  $a'_1$ ) in the ground state  $\sim 2 \, \text{eV}$  apart from each other. If we assume that all bandgap electronic states of NV<sup>-</sup> are formed by excitations within the latter four orbitals, 5 triplet and 10 singlet excited states are conceivable in addition to  ${}^3A_2$ , see Fig. 3.

In the bottom row, we show the occupation patterns where the e and  $a_1$  orbitals are semi- and doubly occupied, respectively. These can be understood as "zeroth-order" excitations, which are expected to

have the lowest energy level among all states. These states are  ${}^3A_2$ ,  ${}^1E$ , and  ${}^1A_1$ .

For first-order excitations, only  $a_1' \to e$  and  $a_1 \to e$  electron jumps are feasible, and the orbital energy gap in the former case is approximately twice smaller. The  $a_1' \to e$  process leads to  ${}^3E$  and  ${}^1E'$ 

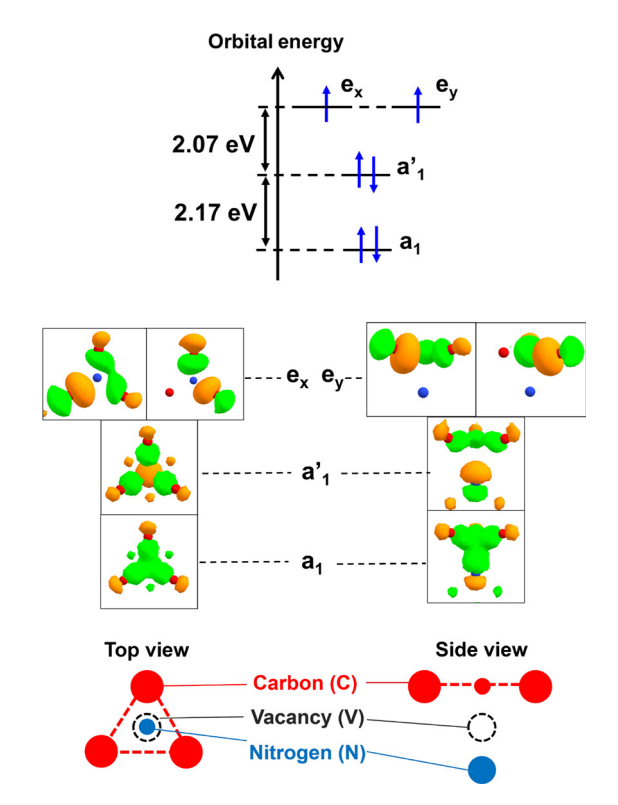


**FIG. 2.** Top: relative energy levels of the defect-localized orbitals of NV<sup>-</sup>, as obtained upon wannierization, i.e., projection of localized spin paired HSE06 orbitals of the supercell model on sp3 states of the nearest neighbor atoms. Bottom: surface plot of the localized bandgap orbitals in the vicinity of the vacancy. Green and orange surfaces indicate positive and negative wavefunction signs, respectively. (Note that CASSCF on cluster models provides similar defect orbital diagram.)

$\begin{array}{c} \text{Triplet states} \\ \text{(S=1)} \end{array}$	$\begin{array}{cc}  ext{Singlet states} \\  ext{(S=0)} \end{array}$			
	## #+ #-  1 A'''	$\begin{array}{c} a_1 \to e \\ a_1 \to e \end{array}$	2nd order excitations	
## #+ + + 3A <sub>1</sub>	## ## + - + + + 1A"	$a_1' \to e \\ a_1 \to e$		
Expected additional states	## - # 1A' <sub>1</sub>	$\begin{array}{c} a_1' \to e \\ a_1' \to e \end{array}$		
$\begin{array}{cccccccccccccccccccccccccccccccccccc$	$\begin{array}{cccccccccccccccccccccccccccccccccccc$	$a_1 \to e$	1st order	
$\begin{array}{cccccccccccccccccccccccccccccccccccc$	$\begin{array}{cccccccccccccccccccccccccccccccccccc$	$a_1' \to e$	excitations	
Spin polarization cycle	$\begin{array}{cccccccccccccccccccccccccccccccccccc$	$e \rightarrow e$	0th order excitations	

**FIG. 3.** Expected electron configurations for the distribution of 6 electrons on the 4 bandgap orbitals according to group theory. The configurations are ordered—from bottom to top—according to the expected energy levels based on the orbital energy diagram.

excited states. Among these,  ${}^3E$  is responsible for the 1.945 eV emission line of NV<sup>-11</sup> and is known to be involved in its spin polarization cycle<sup>10</sup> ( ${}^3A_2 \rightarrow {}^1A_1 \rightarrow {}^1E \rightarrow {}^3A_2$ , highlighted by blue background in Fig. 3). However, the existence of the singlet analog  ${}^1E'$  has only been theoretically predicted to date. One of the singlet analog the group theory indicates that the energy level of  ${}^1E'$  is commensurable with that of  ${}^3E$ , it is reasonable to assume that  ${}^1E'$  is present in the TA spectrum. The  $a_1 \rightarrow e$  transition produces another set of E states, namely,  ${}^3E'$  and  ${}^1E''$ .

We got two triplet and three singlet excited states; however, the three ESA peaks in the singlet TA spectrum indicate that at least one doubly excited singlet state should also be accessible by absorption. Considering the possible second-order excitations, see the top of Fig. 3, energetically the double  $a_1' \rightarrow e$  process is the most favorable. According to the Kohn–Sham orbital picture, the energy demand of a double  $a_1' \rightarrow e$  excitation is similar to a single  $a_1 \rightarrow e$  jump.

Altogether, chemical intuition and group theory strongly suggest that the additional states observed in TA spectroscopy are  $^3E''$ ,  $^1E'$ ,  $^1A'_1$ , and  $^1E''$ . These states are highlighted with red background in Fig. 3. Furthermore, given that only four defect-localized orbitals are present, any other possible distribution of electrons results in double excitations of significantly higher energy.

Now, we test the qualitative predictions of group theory by *ab initio* calculations. Our previously reported initial CASSCF-NEVPT2 results  $^{26}$  indicated that the newly suggested states of  $^3E^{\prime\prime}$ ,  $^1E^{\prime}$ ,  $^1A^{\prime}_1$ , and  $^1E^{\prime\prime}$  are located in the energy range of 3.3–4.6 eV relative to the ground triplet state ( $^3A_2$ ), which correspond well with our present measurement. Herein, we further investigate our hypothesis on  $^3E^{\prime\prime}$ ,  $^1E^{\prime}$ ,  $^1A^{\prime}_1$ , and  $^1E^{\prime\prime}$  states by (i) a comparative analysis of CASSCF-NEVPT2 and cRPA+FCI and (ii) comparing theoretical oscillator strengths from CASSCF-NEVPT2 to the observed relative peak sizes.

As both theoretical approaches take state mixing effects into account, it is worth studying the composition of the eigenstates based on the group theoretically pure configurations of Fig. 3, see Tables S3 and S4 of SI. Strikingly, state mixing effects are observed in all configurations of the singlet channel, in sharp contrast to the triplets where all states were found to be dominated by one configuration. For instance, we observe the previously reported presence of  $^1E^\prime$  in  $^1E$ , which enables the intersystem crossing to  $^3A_2$  as well as the previously reported significant contribution of  $^1A_1^\prime$  to the multireference wavefunction of  $^1A_1$ . We emphasize here that the multireference character of singlets makes the single-determinant methods, such as DFT, highly unreliable for calculating energy differences.

Next, we turn our focus on excitation energies as summarized in Table I, left, and visualized in Fig. 4, see also Tables S1 and S2 of SI for a detailed data analysis. With CASSCF-NEVPT2, we obtain triplet electronic energy levels of 2.11 eV ( ${}^3E$ ) and 4.34 eV ( ${}^3E''$ ), relative to the ground state, which corresponds to absorption peaks of 2.11 eV ( ${}^3A_2 \rightarrow {}^3E$ ) and 2.22 eV ( ${}^3E' \rightarrow {}^3E''$ ), respectively. The results agree well with the experimental peak positions of 1.95 and 2.39 eV. A similarly successful reproduction of the measured energy levels was achieved in the singlet channel, where the excited states are located, compared to the lowest-lying state of  ${}^1E$ , at 1.02 eV ( ${}^1A_1$ ), 2.73 eV ( ${}^1E'$ ), and 3.91 eV ( ${}^1A'_1$ ). The only outlier is the  ${}^1E''$  state with 3.37 eV. Thus, within the measurement limit of <3.3 eV, we predict absorption at 1.02 eV ( ${}^1E \rightarrow {}^1A_1$ ) and 2.73 eV ( ${}^1E \rightarrow {}^1E'$ ) from the ground singlet state while 1.71 eV ( ${}^1A_1 \rightarrow {}^1E'$ ), 2.89 eV ( ${}^1A_1 \rightarrow {}^1A'_1$ ), and 2.35 eV ( ${}^1A_1 \rightarrow {}^1E''$ ) from the first excited singlet.

With cRPA+FCI, the excitation energies in the triplet channel are 2.20 eV ( ${}^3A_2 \rightarrow {}^3E$ ) and 4.55 eV ( ${}^3A_2 \rightarrow {}^3E'$ ). The  ${}^3E \rightarrow {}^3E'$  transition energy is at 2.35 eV. These energies agree very well with both experimental measurements and energies obtained with CASSCF-NEVPT2. For the singlet channel, the excitation energy to the first two states  $({}^{1}A_{1}$  and  ${}^{1}E')$  is at 0.88 and 2.70 eV, respectively. The next state is at 4.49 eV above the lowest singlet state ( ${}^{1}E$ ). This state is the  ${}^{1}A'_{1}$  state, with the  ${}^{1}E''$  state located 0.15 eV above the  ${}^{1}A'_{1}$  state. This is in contrast to the position, ordering and splitting obtained with CASSCF-NEVPT2. The energy splitting of 0.15 eV between  ${}^{1}A'_{1}$  and  ${}^{1}E''$  is reminiscent of the energy splitting between the experimentally observed states at 3.98 and 4.04 eV, but the excitation energy is about 0.5 eV larger than experimentally observed. Furthermore, the  ${}^{1}E''$  state described with cRPA+FCI is more than 1 eV above the value obtained with CASSCF-NEVPT2. The cRPA+FCI method involves certain approximations that may influence the positioning of energy levels. First, the electronic screening is, in this case, computed with the static dielectric function. Furthermore, in the present calculations, there are some double counting errors in the one-body matrix elements (Kohn-Sham energy levels) due to the exchange-correlation energy of the active space, which should be fully included in the two-body matrix

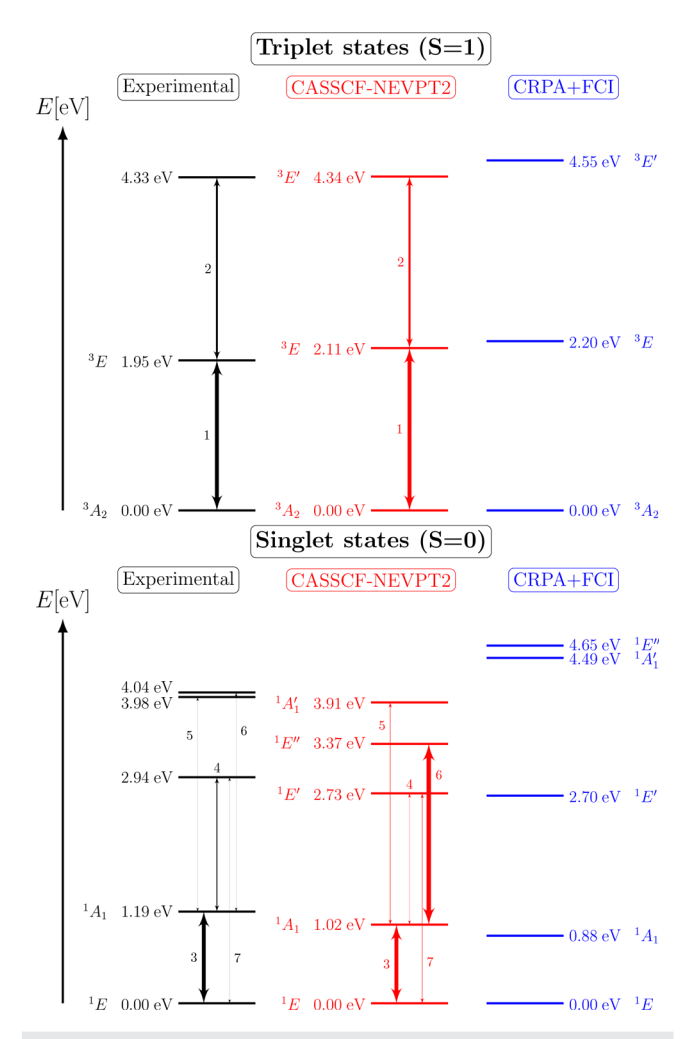


**FIG. 4.** Comparison of experimental (black) and theoretical (red, blue) energy levels of the electronic states of NV $^-$  in triplet (top graph) and singlet (bottom graph) spin states. Experimental levels were calculated from observed ZPL wavelengths, while theoretical values refer to vertical gaps, calculated at CASSCF-NEVPT2 and Cl + CRPA level, respectively (see SI, section S3.1 for a discussion of comparability of the three methods). The thickness of arrows is proportional to the oscillator strength.

elements, but which is neglected in this case. The present cRPA calculation with the considered minimal basis set is qualitatively in agreement with experiments.

Altogether, CASSCF-NEVPT2 predicts the newly identified TA peak positions with less than  $0.2\,\mathrm{eV}$  deviation from the measurement, with the exception of  $^1E''$ , which differs by  $0.5\,\mathrm{eV}$ . This finding is strong evidence for the correctness of our assignment of higher energy states shown in Fig. 3.

Apart from the transition energies, the transition oscillator strength ( $f_{\rm osc}$ ), i.e., absorption cross section, could be used to determine the electronic states (see SI, section S3.2 for details). The calculated oscillator strengths, compared to the experimental integrated peak areas, are provided in Table I. The values are normalized the same way as the experimental ones. In our comparison, we expect only an order-

of-magnitude estimate from theory, given the approximations involved in our methods, and the fact that the experimental values of  $f_{\rm osc}$  are based only on ZPL peaks, even though the Debye–Waller (DW) factor could significantly vary.

In the triplet channel, we find  $f_{\rm osc}=0.54$  for  ${}^3E{\to}^3E'$  at the CASSCF-NEVPT2 level, which is in good agreement with the experimental value of 0.49. In the singlet channel, the peak intensities show more variation. According to our theoretical calculations, after the  ${}^1E{\to}^1A_1$  transition, feature of the TA spectrum is the  ${}^1A_1{\to}^1E'$  transition ( $f_{\rm osc}=0.04$ ), followed by the  ${}^1E{\to}^1E'$  ( $f_{\rm osc}=0.10$ ) and the  ${}^1A_1{\to}^1A'_1$  ( $f_{\rm osc}=0.10$ ) transitions. The deviations of the oscillator strengths from the experimental values, 0.22, 0.01, and 0.01, are tolerable in these cases.

The  $^1A_1 \rightarrow ^1E''$  transition is an exceptional case, where the obtained  $f_{\rm osc}$  value of 1.14 is almost two orders of magnitude higher than the experimental observations. Additionally, the energy of the corresponding transition is in disagreement with the experimental results. This casts some doubt on the identity of one of the peaks at 2.79–2.85 eV, as such a deviation cannot likely be explained by DW-factor variations or by any factor neglected by our computational protocol (e.g., geometry relaxation effects). The potential causes of this discrepancy are discussed in the SI, section S3.3. For the cRPA+FCI calculations, the gauge for the position operator in the Wannier basis does not coincide with the center of charge density, and, hence, the optical matrix elements and consequently the oscillator strengths are not evaluated with this level of theory.

In conclusion, our joint experimental and theoretical study elaborates on the high-energy spectra of the NV center in diamond. Our results, obtained through both TA spectroscopy and advanced computational methods, provide a comprehensive characterization of five high-energy states beyond the commonly studied optical cycle. By combining experimental transition energies and oscillator strengths with theoretical insights from CASSCF-NEVPT2 and cRPA+FCI methods, we not only provide the identification of these states but also deepen our understanding of the NV center's electronic structure.

These findings can have important implications for future applications of NV centers in quantum technologies, particularly in the development of more efficient spin-to-charge conversion readout mechanisms. Additionally, the results we obtained offer a valuable framework for benchmarking high-level first-principles methods in the study of point defects.

See the supplementary material for additional information on the experiments and simulations.

This research was supported by the National Research, Development, and Innovation Office of Hungary within the Quantum Information National Laboratory of Hungary (Grant No. 2022-2.1.1-NL-2022-00004) and Grants FK 135496 and FK 145395. Z.B. also acknowledges the financial support of the János Bolyai Research Fellowship of the Hungarian Academy of Sciences. We acknowledge the support of the European Union under Horizon Europe for the QRC-4-ESP project (Grant Agreement No. 101129663), the QUEST project (Grant Agreement No. 101156088), and funding by the Max-Planck Society. C.L. acknowledges support provided by the Research Council of Norway and the University of Oslo through the research project QuTe (No. 325573, FriPro ToppForsk-program).

The computations were enabled by resources provided by the National Academic Infrastructure for Supercomputing in Sweden (NAISS) and the Swedish National Infrastructure for Computing (SNIC) at NSC, partially funded by the Swedish Research Council through Grant Agreement Nos. 2022-06725 and 2018-05973. We also acknowledge KIFÜ for awarding us computational resources at the Komondor supercomputer in Hungary. In addition, computations were performed on resources provided by UNINETT Sigma2—the National Infrastructure for High Performance Computing and Data Storage in Norway.

## **AUTHOR DECLARATIONS**

#### **Conflict of Interest**

The authors have no conflicts to disclose.

### **Author Contributions**

Minh Tuan Luu, Christopher Linderälv, and Zsolt Benedek contributed equally to this work.

Minh Tuan Luu: Data curation (equal); Formal analysis (equal); Methodology (equal); Writing – original draft (equal); Writing – review & editing (equal). Christopher Linderälv: Methodology (equal); Writing – original draft (equal); Writing – review & editing (equal). Zsolt Benedek: Formal analysis (equal); Methodology (equal); Writing – original draft (equal); Writing – review & editing (equal). Ádám Ganyecz: Formal analysis (equal); Methodology (equal); Writing – original draft (equal); Writing – review & editing (equal). Gergely Barcza: Formal analysis (equal); Methodology (equal); Writing – original draft (equal); Writing – review & editing (equal). Viktor Ivády: Conceptualization (equal); Funding acquisition (equal); Supervision (equal); Writing – original draft (equal); Writing – review & editing (equal). Ronald Ulbricht: Conceptualization (equal); Supervision (equal); Writing – original draft (equal); Writing – review & editing (equal).

# **DATA AVAILABILITY**

The data that support the findings of this study are available from the corresponding author upon reasonable request.

#### **REFERENCES**

- <sup>1</sup>M. W. Doherty, N. B. Manson, P. Delaney, F. Jelezko, J. Wrachtrup, and L. C. Hollenberg, "The nitrogen-vacancy colour centre in diamond," Phys. Rep. **528**, 1–45 (2013).
- <sup>2</sup>C. L. Degen, F. Reinhard, and P. Cappellaro, "Quantum sensing," Rev. Mod. Phys. 89, 035002 (2017).
- <sup>3</sup>J. F. Barry, J. M. Schloss, E. Bauch, M. J. Turner, C. A. Hart, L. M. Pham, and R. L. Walsworth, "Sensitivity optimization for NV-diamond magnetometry," Rev. Mod. Phys. **92**, 015004 (2020).
- <sup>4</sup>N. Aslam, H. Zhou, E. K. Urbach, M. J. Turner, R. L. Walsworth, M. D. Lukin, and H. Park, "Quantum sensors for biomedical applications," Nat. Rev. Phys. 5, 157–169 (2023).
- <sup>5</sup>S. Wehner, D. Elkouss, and R. Hanson, "Quantum internet: A vision for the road ahead," Science 362, eaam9288 (2018).
- <sup>6</sup>G. Balasubramanian, P. Neumann, D. Twitchen, M. Markham, R. Kolesov, N. Mizuochi, J. Isoya, J. Achard, J. Beck, J. Tissler, V. Jacques, P. R. Hemmer, F. Jelezko, and J. Wrachtrup, "Ultralong spin coherence time in isotopically engineered diamond," Nat. Mater. 8, 383 (2009).

- <sup>7</sup>J. Michl, J. Steiner, A. Denisenko, A. Bülau, A. Zimmermann, K. Nakamura, H. Sumiya, S. Onoda, P. Neumann, J. Isoya, and J. Wrachtrup, "Robust and accurate electric field sensing with solid state spin ensembles," Nano Lett. **19**, 4904–4910 (2019).
- <sup>8</sup>G. Kucsko, P. C. Maurer, N. Y. Yao, M. Kubo, H. J. Noh, P. K. Lo, H. Park, and M. D. Lukin, "Nanometre-scale thermometry in a living cell," Nature **500**, 54–58 (2013).
- <sup>9</sup>P. Ovartchaiyapong, K. W. Lee, B. A. Myers, and A. C. B. Jayich, "Dynamic strain-mediated coupling of a single diamond spin to a mechanical resonator," Nat. Commun. 5, 4429 (2014).
- <sup>10</sup>Á. Gali, "Ab initio theory of the nitrogen-vacancy center in diamond," Nanophotonics 8, 1907–1943 (2019).
- <sup>11</sup>A. Gali, E. Janzén, P. Deák, G. Kresse, and E. Kaxiras, "Theory of spin-conserving excitation of the n-v<sup>-</sup> center in diamond," Phys. Rev. Lett. 103, 186404 (2009).
- <sup>12</sup>P. Delaney, J. C. Greer, and J. A. Larsson, "Spin-polarization mechanisms of the nitrogen-vacancy center in diamond," Nano Lett. 10, 610–614 (2010).
- <sup>13</sup>Y. Ma, M. Rohlfing, and A. Gali, "Excited states of the negatively charged nitrogen-vacancy color center in diamond," Phys. Rev. B 81, 041204 (2010).
- <sup>14</sup>S. Choi, M. Jain, and S. G. Louie, "Mechanism for optical initialization of spin in NV" center in diamond," Phys. Rev. B 86, 041202 (2012).
- <sup>15</sup>G. Thiering and A. Gali, "Ab initio calculation of spin-orbit coupling for an NV center in diamond exhibiting dynamic Jahn-Teller effect," Phys. Rev. B 96, 081115 (2017).
- <sup>16</sup>G. Thiering and A. Gali, "Theory of the optical spin-polarization loop of the nitrogen-vacancy center in diamond," Phys. Rev. B 98, 085207 (2018).
- <sup>17</sup>M. Bockstedte, F. Schütz, T. Garratt, V. Ivády, and A. Gali, "Ab initio description of highly correlated states in defects for realizing quantum bits," npj Quant. Mater. 3, 31 (2018).
- <sup>18</sup>H. Ma, M. Govoni, and G. Galli, "Quantum simulations of materials on near-term quantum computers," npj Comput. Mater. 6, 85 (2020).
- <sup>19</sup>C. Bhandari, A. L. Wysocki, S. E. Economou, P. Dev, and K. Park, "Multiconfigurational study of the negatively charged nitrogen-vacancy center in diamond," Phys. Rev. B 103, 014115 (2021).
- <sup>20</sup>N. Sheng, C. Vorwerk, M. Govoni, and G. Galli, "Green's function formulation of quantum defect embedding theory," J. Chem. Theory Comput. 18, 3512–3522 (2022).
- <sup>21</sup>B. A. Barker and D. A. Strubbe, "Spin-flip Bethe-Salpeter equation approach for ground and excited states of open-shell molecules and defects in solids," arXiv:2207.04549 (2022).
- <sup>22</sup>S. Haldar, A. Mitra, M. R. Hermes, and L. Gagliardi, "Local excitations of a charged nitrogen vacancy in diamond with multireference density matrix embedding theory," J. Phys. Chem. Lett. 14, 4273–4280 (2023).
- <sup>23</sup>A. V. Ivanov, Y. L. A. Schmerwitz, G. Levi, and H. Jónsson, "Electronic excitations of the charged nitrogen-vacancy center in diamond obtained using time-independent variational density functional calculations," SciPost Phys. 15, 009 (2023).
- <sup>24</sup>Y. Chen, T. Jiang, H. Chen, E. Han, A. Alavi, K. Yu, E. Wang, and J. Chen, "Multiconfigurational nature of electron correlation within nitrogen vacancy centers in diamond," Phys. Rev. B 108, 045111 (2023).
- 25K. Li, V. D. Dergachev, I. D. Dergachev, S. Zhang, S. A. Varganov, and Y. Ping, "Excited-state dynamics and optically detected magnetic resonance of solid-state spin defects from first principles," Phys. Rev. B 110, 184302 (2024).
- 26Z. Benedek, Á. Ganyecz, A. Pershin, V. Ivády, and G. Barcza, "Accurate and convergent energetics of color centers by wavefunction theory," arXiv:2406.05092 (2024).
- <sup>27</sup>M. Gulka, D. Wirtitsch, V. Ivády, J. Vodnik, J. Hruby, G. Magchiels, E. Bourgeois, A. Gali, M. Trupke, and M. Nesladek, "Room-temperature control and electrical readout of individual nitrogen-vacancy nuclear spins," Nat. Commun. 12, 4421 (2021).
- <sup>28</sup>M.-T. Luu, A. T. Younesi, and R. Ulbricht, "Nitrogen-vacancy centers in diamond: Discovery of additional electronic states," Mater. Quantum Technol. 4, 035201 (2024)
- <sup>29</sup>A. T. Younesi and R. Ulbricht, "Broadband transient absorption spectroscopy using an incoherent white-light source as probe," Opt. Express 30, 38896–38906 (2022).

- 30 A. S. Zyubin, A. M. Mebel, M. Hayashi, H. C. Chang, and S. H. Lin, "Quantum chemical modeling of photoadsorption properties of the nitrogen-vacancy point defect in diamond," J. Comput. Chem. 30, 119–131 (2009).
- <sup>31</sup>J. R. Maze, A. Gali, E. Togan, Y. Chu, A. Trifonov, E. Kaxiras, and M. D. Lukin, "Properties of nitrogen-vacancy centers in diamond: The group theoretic approach," New J. Phys. 13, 025025 (2011).
- <sup>32</sup>M. W. Doherty, N. B. Manson, P. Delaney, and L. C. L. Hollenberg, "The negatively charged nitrogen-vacancy centre in diamond: The electronic solution," New J. Phys. 13, 025019 (2011).
- <sup>33</sup>D. Wirtitsch, G. Wachter, S. Reisenbauer, M. Gulka, V. Ivády, F. Jelezko, A. Gali, M. Nesladek, and M. Trupke, "Exploiting ionization dynamics in the nitrogen vacancy center for rapid, high-contrast spin, and charge state initialization," Phys. Rev. Res. 5, 013014 (2023).
- <sup>34</sup>A. Ranjbar, M. Babamoradi, M. Heidari Saani, M. A. Vesaghi, K. Esfarjani, and Y. Kawazoe, "Many-electron states of nitrogen-vacancy centers in diamond and spin density calculations," Phys. Rev. B 84, 165212 (2011).
- 35W. Pfäffle, D. Antonov, J. Wrachtrup, and G. Bester, "Screened configuration interaction method for open-shell excited states applied to NV centers," Phys. Rev. B 104, 104105 (2021).
- 36P. Siegbahn, A. Heiberg, B. Roos, and B. Levy, "A comparison of the super-CI and the Newton-Raphson scheme in the complete active space SCF method," Phys. Scr. 21, 323 (1980).
- <sup>37</sup>B. O. Roos, P. R. Taylor, and P. E. Sigbahn, "A complete active space SCF method (CASSCF) using a density matrix formulated super-CI approach," Chem. Phys. 48, 157–173 (1980).
- <sup>38</sup>P. E. M. Siegbahn, J. Almlöf, A. Heiberg, and B. O. Roos, "The complete active space SCF (CASSCF) method in a Newton–Raphson formulation with application to the HNO molecule," J. Chem. Phys. 74, 2384–2396 (1981).
- <sup>39</sup>C. Angeli, R. Cimiraglia, S. Evangelisti, T. Leininger, and J.-P. Malrieu, "Introduction of n-electron valence states for multireference perturbation theory," J. Chem. Phys. 114, 10252–10264 (2001).
- <sup>40</sup>C. Angeli, R. Cimiraglia, and J.-P. Malrieu, "N-electron valence state perturbation theory: A spinless formulation and an efficient implementation of the strongly contracted and of the partially contracted variants," J. Chem. Phys. 117, 9138–9153 (2002).
- <sup>41</sup>C. Angeli, M. Pastore, and R. Cimiraglia, "New perspectives in multireference perturbation theory: The n-electron valence state approach," Theor. Chem. Acc. 117, 743–754 (2007).
- <sup>42</sup>L. Muechler, D. I. Badrtdinov, A. Hampel, J. Cano, M. Rösner, and C. E. Dreyer, "Quantum embedding methods for correlated excited states of point defects: Case studies and challenges," Phys. Rev. B 105, 235104 (2022).
- <sup>43</sup>T. H. Dunning, "Gaussian basis sets for use in correlated molecular calculations. I. The atoms boron through neon and hydrogen," J. Chem. Phys. 90, 1007–1023 (1989).
- <sup>44</sup>F. Weigend, "Accurate coulomb-fitting basis sets for H to Rn," Phys. Chem. Chem. Phys. 8, 1057–1065 (2006).
- <sup>45</sup>F. Weigend, A. Köhn, and C. Hättig, "Efficient use of the correlation consistent basis sets in resolution of the identity MP2 calculations," J. Chem. Phys. 116, 3175–3183 (2002).

- <sup>46</sup>F. Neese, "An improvement of the resolution of the identity approximation for the formation of the coulomb matrix," J. Comput. Chem. 24, 1740–1747 (2003).
- <sup>47</sup>F. Neese, F. Wennmohs, A. Hansen, and U. Becker, "Efficient, approximate and parallel Hartree–Fock and hybrid DFT calculations. A 'chain-of-spheres' algorithm for the Hartree–Fock exchange," Chem. Phys. 356, 98–109 (2009).
- <sup>48</sup>B. Helmich-Paris, B. de Souza, F. Neese, and R. Izsák, "An improved chain of spheres for exchange algorithm," J. Chem. Phys. 155, 104109 (2021).
- <sup>49</sup>F. Neese, "Software update: The orca program system, version 5.0," WIRES Comput. Molec. Sci. 12, e1606 (2022).
- <sup>50</sup>C. Kollmar, K. Sivalingam, B. Helmich-Paris, C. Angeli, and F. Neese, "A perturbation-based super-CI approach for the orbital optimization of a CASSCF wave function," J. Comput. Chem. 40, 1463–1470 (2019).
- <sup>51</sup>F. Neese, "The shark integral generation and digestion system," J. Comp. Chem. 44, 1–16 (2022).
- <sup>52</sup>G. Kresse and J. Hafner, "Ab initio molecular-dynamics simulation of the liquid-metal-amorphous-semiconductor transition in germanium," Phys. Rev. B 49, 14251–14269 (1994).
- <sup>53</sup>G. Kresse and J. Furthmüller, "Efficient iterative schemes for ab initio totalenergy calculations using a plane-wave basis set," Phys. Rev. B 54, 11169– 11186 (1996).
- <sup>54</sup>J. Heyd, G. E. Scuseria, and M. Ernzerhof, "Hybrid functionals based on a screened coulomb potential," J. Chem. Phys. 118, 8207 (2003).
- 55J. Heyd, G. E. Scuseria, and M. Ernzerhof, "Erratum: "Hybrid functionals based on a screened coulomb potential" [J. Chem. Phys. 118, 8207 (2003)]," J. Chem. Phys. 124, 219906 (2006).
- 56F. Aryasetiawan, M. Imada, A. Georges, G. Kotliar, S. Biermann, and A. I. Lichtenstein, "Frequency-dependent local interactions and low-energy effective models from electronic structure calculations," Phys. Rev. B 70, 195104 (2004).
- <sup>57</sup>K. Beha, A. Batalov, N. B. Manson, R. Bratschitsch, and A. Leitenstorfer, "Optimum photoluminescence excitation and recharging cycle of single nitrogen-vacancy centers in ultrapure diamond," Phys. Rev. Lett. 109, 097404 (2012).
- <sup>58</sup>R. Ulbricht and Z.-H. Loh, "Excited-state lifetime of the NV-infrared transition in diamond," Phys. Rev. B 98, 094309 (2018).
- <sup>59</sup>A. Gali, M. Fyta, and E. Kaxiras, "Ab initio supercell calculations on nitrogen-vacancy center in diamond: Electronic structure and hyperfine tensors," Phys. Rev. B 77, 155206 (2008).
- <sup>60</sup>J. A. Larsson and P. Delaney, "Electronic structure of the nitrogen-vacancy center in diamond from first-principles theory," Phys. Rev. B 77, 165201 (2008).
- <sup>61</sup>K. Li, V. D. Dergachev, I. D. Dergachev, S. Zhang, S. A. Varganov, and Y. Ping, "Excited-state dynamics and optically detected magnetic resonance of solidstate spin defects from first principles," arXiv:2404.05917 (2024).
- <sup>62</sup>A. Alkauskas, B. B. Buckley, D. D. Awschalom, and C. G. Van de Walle, "First-principles theory of the luminescence lineshape for the triplet transition in diamond NV centres," New J. Phys. 16, 073026 (2014).
- <sup>63</sup>P. Kehayias, M. Doherty, D. English, R. Fischer, A. Jarmola, K. Jensen, N. Leefer, P. Hemmer, N. Manson, and D. Budker, "Infrared absorption band and vibronic structure of the nitrogen-vacancy center in diamond," Phys. Rev. B 88, 165202 (2013).